

# A probabilistic atlas of the human motion complex built from large-scale functional localizer data

Taicheng Huang<sup>1</sup> | Xiayu Chen<sup>1</sup> | Jian Jiang<sup>1</sup> | Zonglei Zhen<sup>2</sup> | Jia Liu<sup>2</sup>

<sup>1</sup>State Key Laboratory of Cognitive Neuroscience and Learning & IDG/McGovern Institute for Brain Research, Beijing Normal University, Beijing, China

<sup>2</sup>Beijing Key Laboratory of Applied Experimental Psychology, National Demonstration Center for Experimental Psychology Education (Beijing Normal University), Faculty of Psychology, Beijing Normal University, Beijing, China

## Correspondence

Zonglei Zhen and Jia Liu, Beijing Key Laboratory of Applied Experimental Psychology, National Demonstration Center for Experimental Psychology Education (Beijing Normal University), Faculty of Psychology, Beijing Normal University, Beijing 100875, China.  
 Emails: zhenzonglei@bnu.edu.cn; liujia@bnu.edu.cn

## Funding information

The National Natural Science Foundation of China, Grant/Award Numbers: 31861143039, 31771251; the National Key R&D Program of China, Grant/Award Number: 2018YFC0810602; the National Social Science Foundation of China, Grant/Award Numbers: 14ZDB160, 15ZDB139; the Changjiang Scholars Program of China

## Abstract

Accurate motion perception is critical to dealing with the changing dynamics of our visual world. A cluster known as the human MT+ complex (hMT+) has been identified as a core region involved in motion perception. Several atlases defined based on cytoarchitecture, retinotopy, connectivity, and multimodal features include homologs of the hMT+. However, an hMT+ atlas defined directly based on this region's response for motion is still lacking. Here, we identified the hMT+ based on motion responses from functional magnetic resonance imaging (fMRI) localizer data in 509 participants and then built a probabilistic atlas of the hMT+. As a result, four main findings were revealed. First, the hMT+ showed large interindividual variability across participants. Second, the atlases stabilized when the number of participants used to build the atlas was more than 100. Third, the functional hMT+ showed good agreement with the hMT+ atlases built based on cytoarchitecture, retinotopy, and connectivity, suggesting a good structural-functional correspondence. Fourth, tests on multiple fMRI data sets acquired from independent participants, imaging parameters and paradigms revealed that the functional hMT+ showed higher sensitivity than all other atlases in ROI analysis except that connectivity and multimodal hMT+ atlases in the left hemisphere could infrequently attain comparable sensitivity to the functional atlas. Taken together, our findings reveal the benefit of using large-scale functional localizer data to build a reliable and representative hMT+ atlas. Our atlas is freely available for download; it can be used to localize the hMT+ in individual participants when functional localizer data are not available.

## KEY WORDS

brain atlas, hMT+, interindividual variability, motion perception, structural-functional correspondence

## 1 | INTRODUCTION

Accurate motion perception is critical to dealing with the changing dynamics of our visual world. Substantial evidence demonstrates that multiple regions are recruited for motion information processing. These visual motion-sensitive regions are often identified by comparing neural responses to moving versus static stimuli in neuroimaging studies (Huk, Dougherty, &

Heeger, 2002; Tootell, Reppas, Dale, et al., 1995; Watson et al., 1993; Zeki et al., 1991). Among them, the most reliable and well-studied regions are located within the lateral occipitotemporal cortex and are commonly referred to as the human MT+ complex (hMT+; DeYoe et al., 1996). It is generally agreed that the hMT+ corresponds to the monkey's middle temporal area (MT or V5), plus a number of neighboring motion-sensitive areas (Amano, Wandell, & Dumoulin, 2009; Kolster, Peeters, & Orban, 2010).

Macroanatomically, the location of the hMT+ has been correlated with a sulcal junction between the inferotemporal sulcus (ITS) and the

Zonglei Zhen and Jia Liu are the co-senior authors.

anterior occipital sulcus (AOS; Figure 1a; Dumoulin et al., 2000). While ITS-AOS junction is prominently identifiable in every brain, it shows morphological variability from one hemisphere to the next (Dumoulin et al., 2000; Malikovic et al., 2007). Moreover, the exact location of the hMT+ relative to the ITS and AOS varies widely among individuals (Duecker et al., 2014; Dumoulin et al., 2000; Malikovic et al., 2007; Van Essen, Glasser, Dierker, Harwell, & Coalson, 2012).

Most brain functional imaging studies have used functional localizers to define the hMT+ in each individual brain and then explore the functional properties of hMT+ across participants. As a result, very little effort has been devoted to building a functional hMT+ atlas that could help characterize the spatial consistency and variability of functional hMT+ among individuals. To the best of our knowledge, only recently have three studies attempted to develop functional probabilistic atlases (or maps) of the hMT+ (Duecker et al., 2014; Frost & Goebel, 2012; Wilms et al., 2005). However, the very small sample size (about 10 participants) used in these studies limited the development of reliable statistical representations of spatial consistency and variability in the hMT+ for whole populations. Therefore, an hMT+ atlas defined by the function criterion, which adequately incorporates hMT+ spatial variability from a large cohort of participants, is still lacking. On the other hand, over the last decade, different other criteria/methods including cytoarchitecture (Malikovic et al., 2007), retinotopy (Wang et al., 2015), connectivity (Fan et al., 2016), and multimodal features (Glasser et al., 2016), have been used to map the areas involved in visual motion processing and to characterize its spatial variability across participants. The hMT+ atlases defined by these criteria show good spatial correspondence, yet with some significant

differences (Figure 1b). However, it is presently unknown whether the hMT+ atlas defined by the function criterion corresponds well with the hMT+ atlases defined based on cytoarchitecture, connectivity, and retinotopy (although they are generally believed to reflect the function of hMT+). A quantitative evaluation of the degree of agreement between a functional hMT+ atlas and other atlases could definitely provide additional information on structural-functional coupling. Finally, it would be interesting to understand whether the functional hMT+ atlas has an advantage over other atlases in extracting hMT+ signals in region of interest (ROI) analysis. Such a feat would be especially useful in patient populations and other groups in which it may be relatively easy to acquire anatomical data, but difficult to acquire functional data. We expect that a well-defined ROI could provide better sensitivity and specificity in extracting hMT+ signals when no individual functional localizer data are acquired.

To address these questions, we implemented a five-fold procedure in 509 participants scanned with a robust hMT+ localizer using the same scanner and MRI protocol. First, we identified the hMT+ in each participant using a customized toolbox. Second, using cortex-based alignment (CBA, Fischl et al., 1999) to transform each hMT+ into a standard space, we built a probabilistic atlas of the functional hMT+ to map the probabilistic location of the hMT+. Third, we examined how the number of participants affected the probabilistic atlas. Fourth, we quantified the spatial correspondence between our functional probabilistic hMT+ atlas and other atlases created using cytoarchitecture (Malikovic et al., 2007), retinotopy (Wang et al., 2015), connectivity (Fan et al., 2016), and multimodal (Glasser et al.,

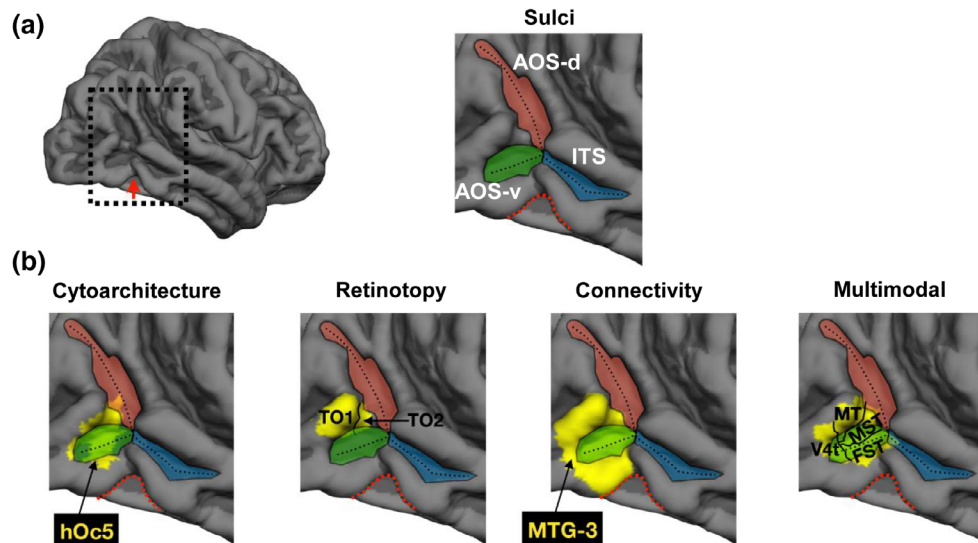


**FIGURE 1** A structural-functional roadmap for the present study. (a) Left: A pial cortical surface reconstruction of the RH from the FS average brain ( $N = 39$  brains; Fischl, Sereno, Tootell, & Dale, 1999; <https://surfer.nmr.mgh.harvard.edu/>). Red arrow: TOI. Right: Zoomed portion of the LOTC as indicated by the dotted square in the left image with sulci defined in different colors: AOS-d (red), AOS-v (green), and ITS (blue). (b) The hMT+ atlases defined using (from left to right): Cytoarchitecture (hOc5; Malikovic et al., 2007), retinotopy (TO-1 and TO-2; Wang, Mruczek, Arcaro, & Kastner, 2015; Amano et al., 2009), connectivity (MTG-3; Fan et al., 2016), and multimodal features (MT/MST/V4t/FST; Glasser et al., 2016). AOS-d, anterior occipital sulcus, dorsal; AOS-v, AOS, ventral; FS, FreeSurfer; hMT+, human motion complex; ITS, inferotemporal sulcus; hOc5, human occipital area 5; LOTC, lateral occipito-temporal cortex; MTG, middle temporal gyrus; RH, right hemisphere; TO, temporal occipital; TOI, TO incisure [Color figure can be viewed at [wileyonlinelibrary.com](http://wileyonlinelibrary.com)]

2016) criteria. Finally, we examined the sensitivity of the different hMT+ atlases in extracting motion-related responses in ROI analysis.

## 2 | METHODS

### 2.1 | Participants

A total of 509 college students (286 females, mean age = 20.31 years,  $SD = 1.26$  years) from Beijing Normal University, China, participated in this study as part of an ongoing project to explore the association among brain organization, cognitive function, and genetics. All participants had normal or corrected-to-normal vision. The study was approved by the Institutional Review Board of Beijing Normal University. All participants gave written informed consent before they took part in the experiment.

### 2.2 | Experimental paradigm

Each participant underwent one functional hMT+ localizer run (336 s) in which moving and stationary concentric rings (3 cycles/ $^\circ$ , visual angle =  $14^\circ$ , viewing distance = 110 cm) were alternatively presented in blocks of 16 s. Low contrast stimuli (8%) were used for greater functional specificity (Tootell, Reppas, Kwong, et al., 1995). The moving concentric rings expanded or contracted with a velocity of  $14^\circ/\text{s}$  (Figure S1, Supporting Information). The run consisted of 21 stimulus blocks, in which the first and last stimulus blocks were stationary rings. During the scan, participants fixated at the center of the screen and passively viewed the stimuli.

### 2.3 | Anatomical imaging and cortical surface reconstruction

#### 2.3.1 | Image acquisition

High-resolution T1-weighted structural MRI images were acquired on a Siemens 3T scanner (MAGNETOM Trio, a Tim system) with a 12-channel phased-array head coil at Beijing Normal University Imaging Center for Brain Research, Beijing, China. The anatomical images were acquired with a magnetization prepared gradient echo sequence and were used to provide anatomical reference (particularly in reference to cortical folding) for the functional scans (repetition time/echo time/inversion time (TR/TE/TI) = 2,530/3.39/1,100 ms, flip angle =  $7^\circ$ , matrix =  $256 \times 256$ , 128 sagittal slices, in-plane resolution =  $1 \times 1 \text{ mm}^2$ , slice thickness = 1.33 mm). Earplugs were used to attenuate scanner noise. A foam pillow and extendable padded head clamps were used to restrain the head motion of participants.

#### 2.3.2 | Cortical surface reconstruction

All anatomical volumes were aligned to the anterior commissure-posterior commissure plane. Using FreeSurfer (FS; <http://surfer.nmr.mgh.harvard.edu>), each anatomical volume was segmented to separate gray from white matter, and the resulting boundary was used to reconstruct the cortical surface for each participant.

## 2.4 | Functional imaging, preprocessing, and general linear model of the functional magnetic resonance imaging time series

### 2.4.1 | Functional image acquisition

Functional magnetic resonance imaging (fMRI) data were acquired with a T2\*-weighted gradient-echo, echo-planar imaging (GRE-EPI) sequence (TR = 2 s, echo time = 30 ms, flip angle =  $90^\circ$ , in-plane resolution =  $3.1 \times 3.1 \text{ mm}^2$ , 30 axial slices, slice thickness = 4.8 mm). As for the anatomical scans, earplugs were used to attenuate scanner noise and a foam pillow and extendable padded head clamps were used to restrain the head motion of participants.

### 2.4.2 | Preprocessing

Statistical analyses of functional data were performed with the FS Functional Analysis Stream (<https://surfer.nmr.mgh.harvard.edu>). All functional images from individual participants were preprocessed with motion correction, brain masking, and grand-mean intensity normalization. No spatial smoothing was performed. The preprocessed individual functional data were aligned and resampled to the native cortical surface using a rigid transform with 6 degrees of freedom, which were computed from a boundary-based registration algorithm (Greve & Fischl, 2009).

### 2.4.3 | General linear model of the fMRI time series

Functional data were regressed vertex by vertex with a general linear model (GLM) in which the time series of the moving concentric rings were modeled as a convolution of a boxcar with a canonical hemodynamic response function. The stationary concentric rings were considered as the baseline and not explicitly modeled. In order to reduce the influence of head motion, the six head motion measurements that were generated from the motion correction were also included in the GLM.

## 2.5 | Motion-responsive maps and ROI delineation

### 2.5.1 | Motion-responsive maps

Motion-responsive maps were computed by comparing fMRI responses during blocks of moving rings to fMRI responses from the baseline (i.e., the blocks of static rings). This comparison was conducted at the level of each vertex and summarized into a Z-statistic to generate a motion-responsive map across vertices. Motion-responsive vertices were identified by thresholding this map with a significance value of  $Z > 3.3$  ( $p < .001$ ).

### 2.5.2 | hMT+ delineation

hMT+ was identified within the cortical surface reconstructions of 1,018 individual hemispheres. Once the motion contrast map (moving vs. static ring) was thresholded in each hemisphere, the identification of hMT+ was performed on the thresholded map by taking the anatomical landmark and the appearance of activation clusters (i.e., location, height,

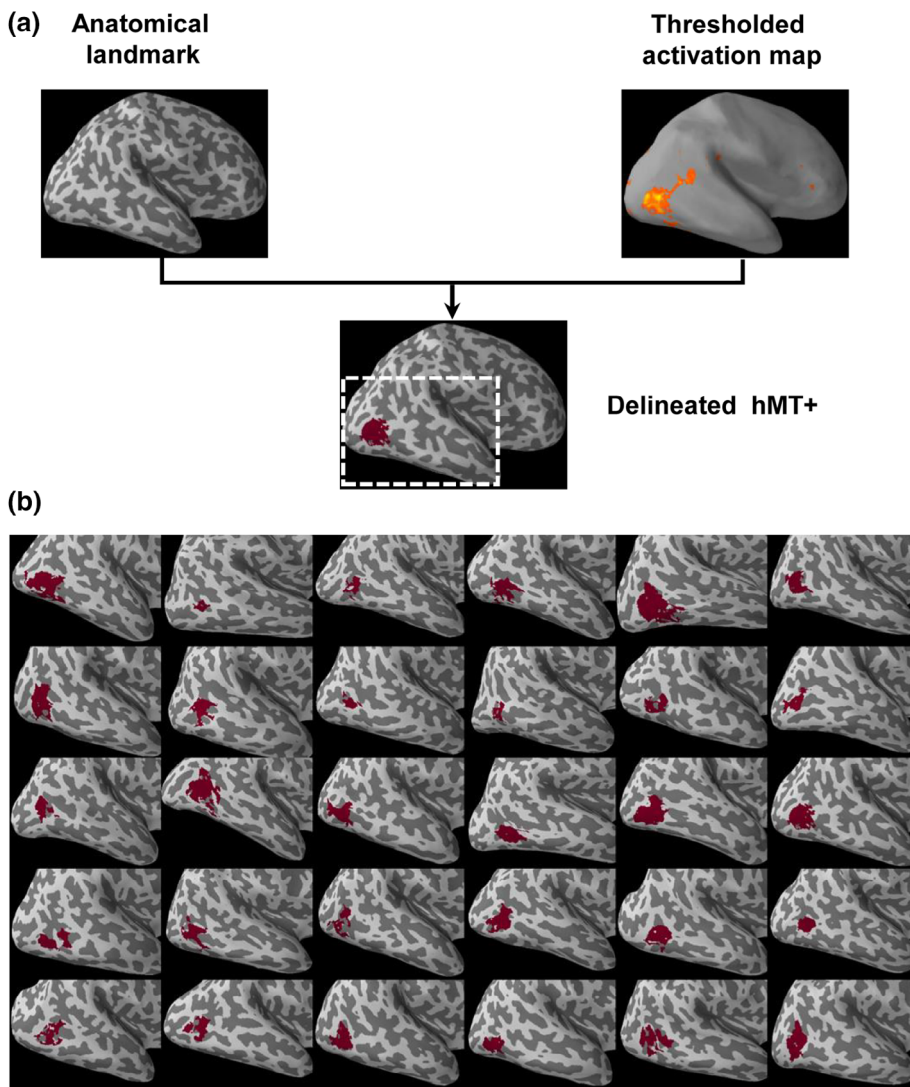


**FIGURE 2** The framework for delineating the hMT+. (a) Top: The hMT+ was identified separately from the cortical surface reconstruction of each participant using the intersection of the AOS and ITS as an anatomical landmark to identify the cortical neighborhood of the hMT+. Bottom: The hMT+ was defined within each individual hemisphere. (b) Inflated cortical surfaces of the RH from 30 participants chosen at random from our large group of participants. The portion of the cortical surface that is depicted is zoomed on the LOTC. The perimeter of the zoomed portion is delineated by the dotted white rectangle in (a). The reader can appreciate the individual differences in the size, shape, and exact relationship of the hMT+ relative to the AOS and ITS. See Figure S2, Supporting Information for the delineations in the LH. AOS, anterior occipital sulcus; hMT+, human motion complex; ITC, inferotemporal sulcus; LOTC, lateral occipito-temporal cortex; LH, left hemisphere; RH, right hemisphere [Color figure can be viewed at [wileyonlinelibrary.com](http://wileyonlinelibrary.com)]

and extent) into account (Figure 2). As a reliable coupling between the ITS-AOS junction and hMT+ was well established at the centimeter scale (Dumoulin et al., 2000; Figure 1), we used the ITS-AOS junction as the landmark to constrain the anatomical neighborhood of hMT+. Then, the activation clusters, which were located closely to the landmark and contiguous on the cortical surface, were handpicked by one rater (T.H.) to construct the individual hMT+. The contiguous clusters with peaks distant from ITS-AOS junction ( $>2$  cm) were excluded. For a contiguous cluster which had multiple peaks, only the sub-clusters whose peaks located nearby ITS-AOS junction were included. Note that all decisions were made by the rater adaptively as it was hard to set some fixed quantitative inclusion/exclusion criteria for a cluster. Finally, the identified hMT+ from each of the participants was verified for accuracy and approved by Z.Z. The FreeROI toolbox (<http://freeroi.brainactivityatlas.org>) was used for the delineations.

## 2.6 | Generation of the hMT+ probabilistic atlas

Individual hMT+ ROIs could be defined in 478 participants (93.9%) in the left hemisphere (LH) and 483 participants (94.9%) in the right

hemisphere (RH). The stability of the time course within each individual ROI was measured by temporal signal-to-noise ratio (tSNR), which was calculated by dividing the mean of residuals by its SD after removing task signal and nuisance regressors (Bennett & Miller, 2010). To avoid the influence from the participants who showed low tSNR, we build the probabilistic hMT+ atlas using the first half of participants (LH:  $N = 239$ ; RH:  $N = 241$ ) who had high tSNR within their individual hMT+ by implementing the following three methodological steps. First, each participant's native cortical surface was spatially normalized to the FS average template by using a high-dimensional nonlinear CBA technique (Fischl et al., 1999). Second, each participant's hMT+ was converted from each individual surface to the standard FS average surface using nearest-neighbor interpolation. Third, a probabilistic hMT+ map was calculated by summing the ROIs at each vertex along the cortical surface of the FS average brain and dividing by the number of participants. Consequently, each vertex in the map represents the frequency of the hMT+ being presented at a given position on the FS average brain across all participants. Together, the map provides a vertex-wise description for both the consistency (e.g., a high proportion of participants at a given vertex would indicate

a high convergence of the hMT+ at that anatomical location) and interindividual variability (e.g., a low proportion of participants at a given vertex would indicate a low convergence of the hMT+ at that anatomical location) in the location and extent of hMT+.

## 2.7 | Reliability of the probabilistic hMT+ atlas

Ample sample size is a prerequisite for building an atlas with good reliability. To assess if the sample size we used was enough to produce a reliable atlas of the hMT+, a two-stage randomization procedure was implemented. Specifically, our participant pool was first split into two halves randomly. Then, several subgroups containing a specific number of participants were randomly generated from each split, and for each group, the number of participants ranged from 3 to 117 (in steps of three participants). We used the dice coefficient to quantify the spatial correspondence between the probabilistic atlases from two subgroups in which 0 indicates no correspondence and 1 indicates perfect correspondence. The dice coefficient is calculated with the following formula:

$$\text{Dice coefficient} = \frac{2 * |A \cap B|}{|A| + |B|}.$$

where A is the surface area of a probabilistic hMT+ ROI and B is the surface area of another probabilistic hMT+ ROI. To alleviate random bias, we repeated the subgroup generation 20 times. The mean and SD of the dice coefficient was finally calculated for each subgroup across all pairs of samples.

## 2.8 | Spatial correspondence between the functional hMT+ atlas and the hMT+ atlases defined by other criteria

We examined the spatial correspondence between the functional hMT+ atlas and previously published hMT+ atlases. Specifically, the cytoarchitectonic hMT+ (or hOc5) atlas was collected from the JuBrain atlas, which was built by an observer-independent cytoarchitectonic analysis procedure (Malikovic et al., 2007). The topological hMT+ atlas was extracted from a visual topography atlas (Wang et al., 2015), which was created by the retinotopic mapping procedure: the TO1 (i.e., MT) and TO2 (i.e., MST) labels from this atlas were merged as the topological hMT+ as previous studies show good correspondence between these regions and hMT+ (Amano et al., 2009). The connectivity-based hMT+ (or middle temporal gyrus [MTG-3]) atlas was collected from the Brainnetome Atlas, which was created by an automatic parcellation procedure on the anatomical connection patterns of each area (Fan et al., 2016). Finally, we combined the areas MT, MST, V4t, and FST in multimodal parcellation atlas from the Human Connectome Project (HCP) as the multimodal hMT+ (Glasser et al., 2016) because previous research has shown that the hMT+ consists of these four regions defined retinotopically (Kolster et al., 2010). As these parcellations have been aligned and shared to the FS average template (Figure 1), we directly quantified the spatial correspondence between the functional

hMT+ atlas and each of the four other atlases at the group level using the dice coefficient.

Since the probabilistic hMT+ maps created by different criteria were distinct in both shape and size, a titration procedure was developed to avoid possible biases from a fixed area size in measuring their spatial correspondence to the functional hMT+. That is, we measured the spatial correspondence among atlases on a wide range of area sizes from 100 vertices to 1,500 vertices (step size = 100) in fsaverage surface. Specifically, for each area size, atlas-specific hMT+ was defined with a region-growing algorithm which used the global maximum probability of each probabilistic map as the seed and then grew regions by incorporating neighboring vertices, one vertex at a time, in decreasing order of probability value, until reaching the specified area size. Finally, for easy evaluation, the area sizes were converted from vertices number to physical size ( $\text{mm}^2$ ) based on the fsaverage surface shape in further statistical analysis.

## 2.9 | Interhemispheric spatial correspondence of hMT+ atlases

To measure the interhemispheric correspondence of each hMT+ atlas, we first registered the atlases on both hemispheres to the "fsaverage\_sym" symmetric surface template using the surface-based interhemispheric registration (Greve et al., 2013). Then, we measured the interhemispheric correspondence of each atlas using the dice coefficient. The same titration procedure as that used in measuring the spatial correspondence between atlases was adopted to avoid possible biases from a fixed area size.

## 2.10 | The sensitivity of the hMT+ atlas in extracting motion-related responses

Three levels of analyses were conducted based on three different data sets to test the performance of the functional hMT+ atlas in extracting motion-related neural responses in individual participants. Each of the hMT+ atlases were aligned to the individual space through surface-based registration and used to extract the motion-related response from these data sets. Specifically, the motion-related response of a vertex was defined as the percentage signal change (PSC) for the contrast between moving stimuli and static stimuli. The PSC for an hMT+ ROI was calculated as the mean of PSC values across all vertices within the ROI. The same titration procedure as that used in measuring correspondence of the atlases was adopted to avoid possible biases from a fixed area size.

First, we used the fMRI data from the second half of participants ( $N = 240$ ), who were excluded from the generation of the functional hMT+ atlas because of relatively low tSNR, to examine the performance of hMT+ atlases in extracting motion-related responses. Note that despite this data set was not independent of the data used to build functional hMT+ in stimuli and imaging parameters, it was independent in participants. Thus, this analysis is helpful to illustrate if the functional hMT+ atlas could generalize well to independent participants with an identical experimental setting.

Second, we tested the performance of hMT+ atlases in an fMRI data set from independent participants and stimuli. An fMRI data set originally collected to localize category-selective areas was used (Zhen et al., 2015). Participants ( $N = 233$ ) were scanned three blocked-design runs (lasted 198 s) in which dynamic movie stimuli (faces, scenes, objects, and scrambled objects) were presented alternately with static fixation. Each run contained two block sets, intermixed with three 18-s rest blocks at the beginning, middle, and end of the run. Each block set contained one 18-s block for each of the four stimulus categories. During scanning, subjects were instructed to view movie clips passively. The fMRI data were acquired from the same scanner and imaging protocol (i.e., parameters) and preprocessed with the same pipeline as the hMT+ localizer data set. The motion-related response was calculated as the PSC for the contrast of moving videos and fixations.

Finally, we tested the performance of hMT+ atlases in an fMRI data set from independent participants, tasks, and imaging parameters. We used the social cognition task fMRI data from HCP ( $N = 1,050$ ), which were scanned alternately under a dynamic movie and static fixation with high temporal and spatial resolutions. In this task, two kinds of moving stimuli were presented by short video clips (20 s) of objects (squares, circles, triangles): the objects dynamically interact (move) in some way (mental interaction) or randomly (random interaction) (Castelli, Happe, Frith, & Frith, 2000; Wheatley, Milleville, & Martin, 2007). Two fMRI runs were conducted in each participants using a multiband EPI sequence (TR = 720 ms, TE = 33.1 ms, flip angle = 52°, voxel size =  $2 \times 2 \times 2$  mm $^3$ ). Each run consisted of five video blocks and five fixation blocks (15 s each). The data were preprocessed with the HCP fMRISurface pipeline and the beta map for each condition was produced and mapped to the standard CIFTI grayordinates space. More details of the HCP data acquisition protocols and preprocessing can be found elsewhere (Barch et al., 2013; Glasser et al., 2013). The motion-related response was calculated as the PSC for the contrast of moving videos and fixations.

### 3 | RESULTS

#### 3.1 | The probabilistic functional hMT+ atlas shows good convergence in the AOS but large interindividual variability outside the AOS

Based on the functional motion localizer data set collected from 509 participants with conventional spatiotemporal resolution (TR = 2 s, voxel size =  $3.1 \times 3.1 \times 4.8$  mm $^3$ ), we manually identified the hMT+ using both macroanatomical and functional information in individual participants. Under the significance threshold of  $p < .001$  ( $Z > 3.3$ ), the hMT+ was successfully delineated in nearly all our 509 participants (LH: 93.9%,  $N = 478$ ; RH: 94.9%,  $N = 483$ ; Figure 2b and Figure S2, Supporting Information). Fifty-seven hemispheres had no hMT+ defined on them because no activation vertices survived the thresholding (39 hemispheres) or no survived vertices met the anatomical criteria (18 hemispheres) for hMT+ delineation. To alleviate the influence from the data with low tSNR, the first half of

participants who had high tSNR within their hMT+ (LH:  $N = 239$ ; RH:  $N = 241$ ) were used to build the probabilistic hMT+ atlas (see Figure S3, Supporting Information, for the distribution of tSNR). From these individual ROIs, we generated an hMT+ probabilistic map (Figure 3a) by: (a) using CBA to project each individual hMT+ ROI to the FS average surface, (b) summing the frequency of hMT+ at each vertex across participants, and (c) dividing the frequency by the number of participants. As such, each vertex within the map reflects the percentage of participants exhibiting motion responses at that location. The probabilistic hMT+ converged well in the center and extended vertically to the ITS. The highest convergence (LH: 80.8%; RH: 80.6%) occurred within the ventral portion of the AOS. On the other hand, relatively large interindividual variability was found outside the AOS. The convergence decreased much from the center vertices to the outer vertices: 50% vertices appeared in less than six and nine participants in LH and RH, respectively. Further analysis revealed that these variabilities could originate from both shifts in the location of activation peaks and changes in the area in individual hMT+. As shown in Figure 3b, the locations of peak activation spread much within the atlas. Again, the area of individual hMT+ varied substantially among participants (Figure 3c). These findings were replicable when using the second half of participants who had relatively low tSNR (Figure S4, Supporting Information) or using stricter activation thresholds (Figure S5, Supporting Information) to generate the atlas.

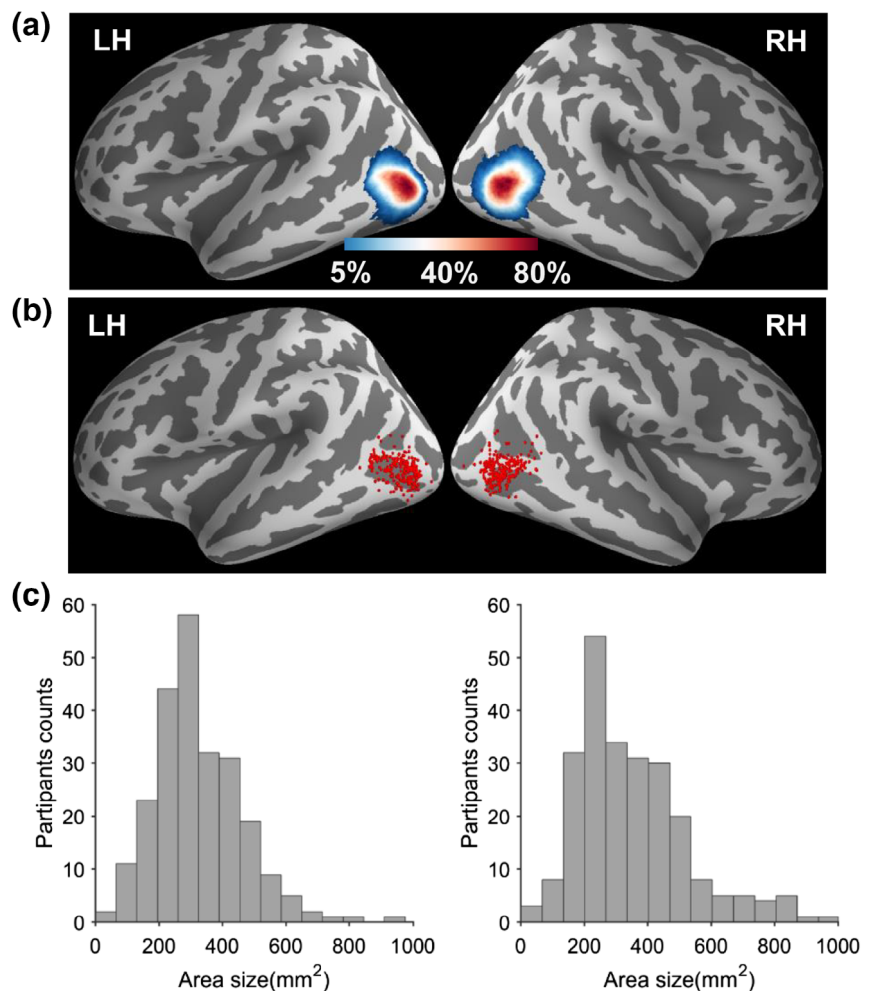
#### 3.2 | The benefit of a large sample size for generating a stable, probabilistic hMT+ map

Sufficiently large sample size is necessary to build an hMT+ atlas with good representativeness. For this, a two-stage randomization procedure was used to evaluate how the reliability of the hMT+ probabilistic atlas varied over the number of participants. Two main findings were revealed (Figure 4). First, small numbers of participants were not enough to replicate the pattern of the probabilistic atlas. The dice coefficient between two independent groups was only about 0.80 when 10 participants were used but reached 0.90 when more than 60 participants were used. Second, the spatial correspondence between the hMT+ probabilistic maps from the two subgroups stabilized at a dice coefficient of about 0.94, when the number of participants was more than 100. These results demonstrated that the sample size of our present study was sufficiently large to create a stable probabilistic hMT+ atlas from about 240 participants.

#### 3.3 | The functional hMT+ shows good spatial correspondence to hMT+ defined by other criteria

Till date, cytoarchitecture (Malikovic et al., 2007), retinotopy (Wang et al., 2015), connectivity (Fan et al., 2016), and multimodal features (Glasser et al., 2016) criteria have been used to delineate hMT+. Figure 5a illustrates our functional hMT+ atlas (red contour) relative to each of the other atlases. We quantified the spatial correspondence between the functional hMT+ and each of the four other hMT+ using the dice coefficient (Figure 5b). This approach revealed three findings.

**FIGURE 3** The definition of the human motion complex (hMT+) atlas. (a) Probabilistic hMT+ atlas of the left and right hemisphere on the FreeSurfer (FS) average surface calculated from participants with high temporal signal-to-noise ratio (tSNR). Each participant's binary hMT+ was first spatially normalized to the FS average surface and then the probabilistic hMT+ map was calculated by summing the individual hMT+ at each vertex and dividing by the number of participants. Finally, for visualization, the map was thresholded to reflect those voxels that are shared by at least 25 participants (i.e., 5%). (b) The location of individual peak activation within the hMT+ was distributed widely across participants with high tSNR. Each dot corresponds to one participant. The individual's peak activation locations were extracted after the individual activation maps were normalized to the FS average surface. (c) The size of individual hMT+ varied greatly across participants. A significance threshold of  $p < .001$  ( $Z > 3.3$ ) was used to define the hMT+ in each participant, and the individual hMT+ size was measured after the individual activation map was normalized to the FS average surface. LH, left hemisphere; RH, right hemisphere [Color figure can be viewed at [wileyonlinelibrary.com](http://wileyonlinelibrary.com)]



First, the hMT+ defined by other criteria generally agreed well with functional hMT+ when the area sizes were larger than 200 mm<sup>2</sup> (dice coefficient  $>0.6$ ). The agreements were relatively poor when areas

were small (i.e., at the center). Second, the correspondences varied greatly across different atlases. The multimodal hMT+ showed the tightest correspondence to the functional hMT+ compared to other

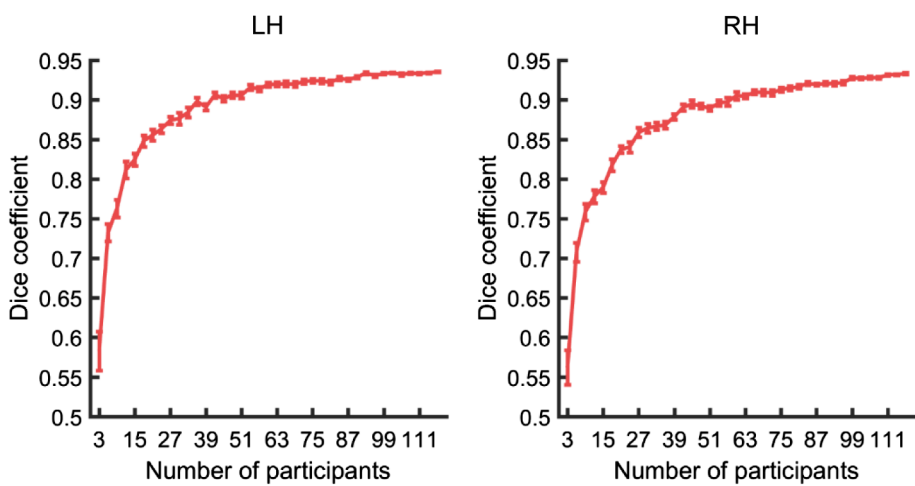


**FIGURE 4** The effect of sample size in the generation of the hMT+ atlas. We implemented a two-stage randomization procedure to assess the stability of the resulting probabilistic hMT+ atlas from subgroups that varied based on the number of participants. The number of participants ranged from 3 to 117 in steps of three participants. The dice coefficient between the probabilistic atlases from the two subgroups was calculated as the stability of the resulting probabilistic atlas. To each number of participants, we iterated 20 times to show its random bias. Mean and SD are plotted in this figure. hMT+, human motion complex; LH, left hemisphere; RH, right hemisphere [Color figure can be viewed at [wileyonlinelibrary.com](http://wileyonlinelibrary.com)]

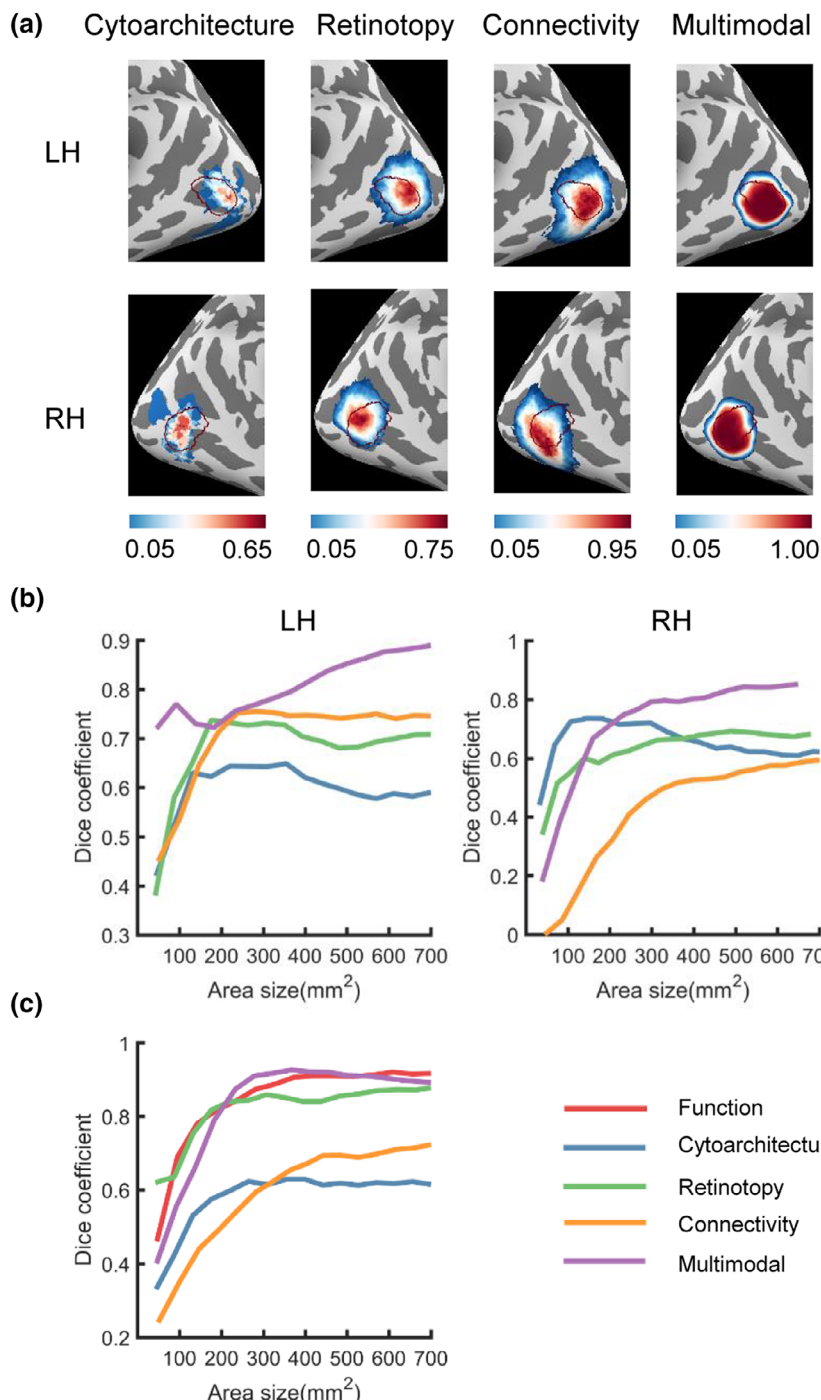


**FIGURE 5** The spatial correspondence between the functional human motion complex (hMT+) atlas and previously published hMT+ atlases. (a) The contour (red) of the hMT+ atlas was plotted relative to recently published probabilistic anatomical and functional hMT+ atlases. From left to right: Cytoarchitecture ( $N = 10$ , Malikovic et al., 2007), retinotopy ( $N = 53$ , Wang et al., 2015), connectivity ( $N = 40$ , Fan et al., 2016), and multimodal ( $N = 210$ , Glasser et al., 2016). For visual comparison, the color range was adjusted specifically for each atlas. (b) The correspondence between each parcellation relative to the hMT+ atlas was assessed using the dice coefficient. To avoid the possible biases from a fixed area size to define hMT+, the spatial correspondence among atlases were measured on a wide range of area sizes from  $100 \text{ mm}^2$  to  $700 \text{ mm}^2$  on fsaverage surface. The multimodal hMT+ showed the highest correspondence with the functional hMT+ atlas, which was consistent across the two hemispheres. (c) The interhemispheric correspondence of each parcellation was assessed using the dice coefficient. In measuring the interhemispheric correspondence of each hMT+ atlas, the atlases on both hemispheres were registered to the "fsaverage\_sym" symmetric surface. the interhemispheric correspondences of each hMT+ atlas were measured on a wide range of area sizes from  $100 \text{ mm}^2$  to  $700 \text{ mm}^2$  on fsaverage surface to avoid the possible biases from a fixed area size. The functional, retinotopic and multimodal hMT+ showed significant interhemispheric correspondence, while cytoarchitectural and connectivity hMT+ showed poor interhemispheric correspondence. LH, left hemisphere; RH, right hemisphere [Color figure can be viewed at [wileyonlinelibrary.com](http://wileyonlinelibrary.com)]

hMT+, especially at surface areas above  $300 \text{ mm}^2$  with dice coefficients  $>0.8$ . Finally, the retinotopic and multimodal hMT+ had similar correspondences to the functional hMT+ in the two hemispheres whereas hMT+ atlases from both cytoarchitectural and connectivity criteria showed significant interhemispheric differences in their correspondences to the functional hMT+. The former showed more correspondence to the functional hMT+ in LH than that in RH whereas the latter showed the opposite behavior. To uncover the possible reasons of these significant interhemispheric differences in the correspondences to the functional hMT+, we registered the atlases on both hemispheres to the "fsaverage\_sym" symmetric template and measured the interhemispheric

correspondence of each atlas. We found that the functional, retinotopic, and multimodal hMT+ showed good interhemispheric correspondences (Figure 5c). When the area sizes were larger than  $200 \text{ mm}^2$ , their interhemispheric correspondences reached 0.9. On the contrary, the connectivity and cytoarchitectonic hMT+ showed relatively poor interhemispheric correspondences. Their interhemispheric correspondences showed a value of 0.65 when the area sizes were larger than  $200 \text{ mm}^2$ . This explains why these two atlases showed different correspondences to the functional hMT+ in the two hemispheres. Together, these results indicated that although the functional hMT agreed well to hMT+ defined by other criteria, it had unique features.

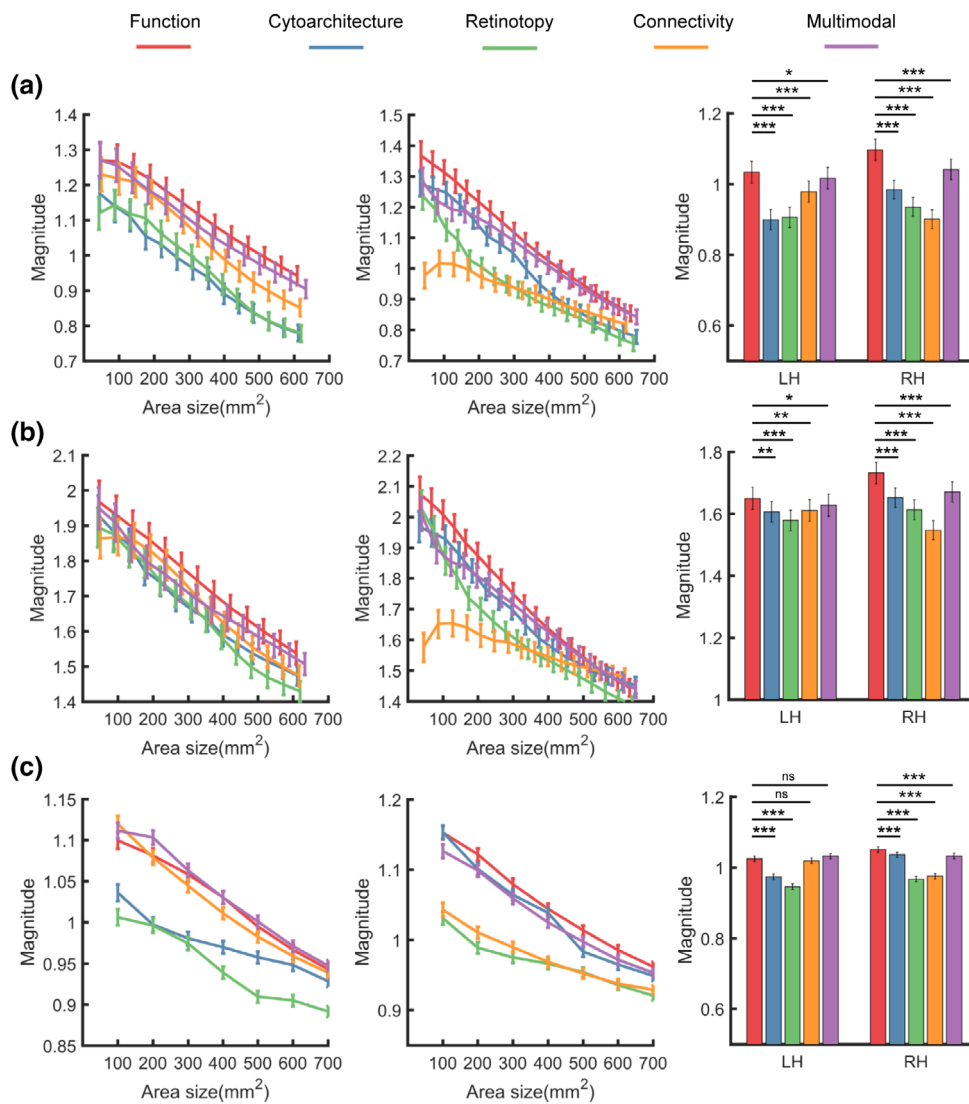


**FIGURE 6** The functional hMT+ shows higher sensitivity in extracting motion-related responses compared to other hMT+ atlases. The amplitude of motion-related responses is plotted as a function of area size for both the left and RH for functional, cytoarchitectonic, retinotopic, connectivity, and multimodal hMT+ atlases. (a) The magnitude of motion-related responses (mean  $\pm$  SEM) extracted from an independent group of participants scanned with the same functional localizer as that used in generating the functional hMT+ (left and middle columns). Paired t tests on the mean magnitude across different area sizes (x axis) revealed that the motion-related responses from the functional hMT+ atlas were larger in magnitude than that from all other hMT+ atlases (right column). (b) The magnitude of motion-related responses (mean  $\pm$  SEM) extracted from dynamic object localizer fMRI data, which were independent of participants and task (left and middle columns). Paired t tests on the mean magnitude across different area sizes (x axis) revealed that the motion-related responses from the functional hMT+ atlas showed the largest magnitude among all atlases (right column). (c) The magnitude of motion-related responses (mean  $\pm$  SEM) extracted from the social cognition task fMRI data from the HCP with independent participants, stimuli, and imaging parameters (left and middle columns). Paired t tests on the mean magnitude across different area sizes (x axis) revealed that the sensitivity of the functional hMT+ atlas was superior to that of the other three atlases except for connectivity and multimodal hMT+ in the LH (right column). fMRI, functional magnetic resonance imaging; HCP, Human Connectome Project; hMT+, human motion complex; LH, left hemisphere; RH, right hemisphere. Two-tailed, Bonferroni corrected: \* $p < .05$ . \*\* $p < .01$ . \*\*\* $p < .001$ . ns, not significant [Color figure can be viewed at [wileyonlinelibrary.com](#)]

### 3.4 | The functional hMT+ atlas shows higher sensitivity in extracting motion-related responses than the hMT+ atlases based on other criteria

As shown above, marked differences were found between the functional hMT+ and the hMT+ based on other criteria. Next, we examined whether these differences mattered in ROI analysis for extracting motion-related neural responses in individual participants. For this,

three levels of analyses were conducted based on three data sets which were distinct from the fMRI data used to generate the functional hMT+ atlas in participants, stimuli, or imaging parameters. The titration procedure was also adopted to avoid possible biases from a fixed area size. First, we used the motion localizer data from the second half of participants ( $N = 240$ ) to test how well each atlas could generalize to the fMRI data which were acquired in independent participants with the identical

task and imaging parameters as the functional hMT+ atlas. We found that the motion-related responses from the functional hMT+ showed the highest magnitude among all five hMT+ atlases (Figure 6a). Second, we tested the performance of hMT+ atlases in an fMRI data set acquired from independent participants ( $N = 233$ ) and task (i.e., a dynamic object localizer) with the same imaging parameters as the motion localizer. Again, the motion-related responses from the functional hMT+ showed the highest magnitude among all five hMT+ atlases (Figure 6b). Finally, we used hMT+ atlases as ROIs to extract motion-related responses from the HCP social cognition task fMRI data ( $N = 1,050$ ). The data set was independent of the hMT+ functional localizer in participants, task, and imaging parameters. We found that the sensitivity of the functional hMT+ atlas in extracting motion-related responses was superior to all atlases except to the connectivity and multimodal hMT+ in the LH where it showed comparable sensitivity (Figure 6c). Taken together, these results demonstrated that the functional hMT+ atlas had higher or comparable sensitivity in extracting motion-related responses in independent participants than other atlases regardless of whether the target data set was acquired with the same stimuli and imaging parameters. Another interesting finding is that the multimodal hMT+ consistently showed the highest sensitivity after the functional hMT+ and even had comparable sensitivity to the functional hMT+ in the LH for the HCP data set.

## 4 | DISCUSSION

In this study, we built a probabilistic hMT+ atlas based on the function criterion from large-scale functional localizer data. Our results revealed four main findings. First, the individual hMT+ converged well to the ventral portion of the AOS but also showed large interindividual variability in its center and size. Second, reliable probabilistic localization was reached when data from 100 participants were used. Third, the functional hMT+ atlas showed good correspondence with the hMT+ atlas defined based on cytoarchitecture, retinotopy, and connectivity, with the tightest correspondence with the multimodal hMT+ atlas. Fourth, comparison analyses on multiple independent fMRI data sets demonstrated that the functional hMT+ was superior to all other atlases in extracting motion-related response for ROI analysis with few exceptions that connectivity and multimodal atlases reached similar sensitivity to the functional atlases.

### 4.1 | Large interindividual variability of the functional hMT+

Our functional hMT+ atlas, which was built based on a large cohort of participants, revealed that functional hMT+ varied much in its peak and size across participants (Figure 3). Such a large interindividual variability had also been found previous studies (Bridge, Clare, & Krug, 2014; Engell & McCarthy, 2013; Large et al., 2016). The variability may stem from multiple sources. First, the large interindividual variability may arise from the functional plasticity of the brain. Previous studies have revealed individual experiences in the early (Golarai et al., 2007) and even late years (Gauthier, Curran,

Curby, & Collins, 2003; Polley, Steinberg, & Merzenich, 2006; Song, Hu, Li, Li, & Liu, 2010) of development may cause a displacement of the brain regions and an increase or decrease of region size, possibly as a result of cortical competition. Second, a growing body of evidence indicates that individual variations in brain activation are significantly modulated by genetic factors (Blokland et al., 2011; Koten Jr. et al., 2009; Polk, Park, Smith, & Park, 2007). Indeed, these studies revealed that the contribution of genetics is larger than that of the environment in shaping brain activations. Finally, the large variability of hMT+ is likely to be a joint outcome of genetic and environmental factors. Nature and nurture are not simply additive interactions that result in a particular appearance of brain areas, but rather a complex interplay of many factors. To what extent the variability of functional regions is determined by nurture, nature, and their interactions requires further investigation.

What cognitive mechanism does the interindividual variability of hMT+ reflect is another fascinating question. One possibility is that the interindividual variability of hMT+ is partially from interindividual differences in the attention or eye movement in the scanning. To test this hypothesis, we examined how the interindividual variability of activities from the hMT+ could be explained by the activities from the attention or eye movement areas. We extracted the response (moving vs. stationary) of the intraparietal sulcus (IPS) and frontal eye field (FEF) using the corresponding ROIs from the retinotopic atlas (Wang et al., 2015), and calculated the correlation of responses from the hMT+ and IPS/FEF across participants whose data were used to generate our functional hMT+ atlas. We found that the individual differences in the responses of IPS were significantly correlated with that from the hMT+ (LH:  $r = .24$ , Bonferroni corrected  $p < .001$ ; RH:  $r = .32$ , Bonferroni corrected  $p < .001$ ), whereas FEF showed no correlation with the hMT+ in individual differences (Bonferroni corrected  $ps > .05$ ) (Figure S6, Supporting Information). This suggests that the interindividual variability of the hMT+ could be partially accounted for by the attention.

### 4.2 | Structural-functional coupling in the hMT+

It is generally believed that there is a coupling between anatomical (e.g., cortical folding, cytoarchitecture, and white matter connections) and functional organization (e.g., retinotopy and functional responses). Recent methodological advancements have improved our understanding of the coupling in the hMT+ through *in vivo* multimodal imaging of the individual brain (Duecker et al., 2014; Dumoulin et al., 2000; Van Essen et al., 2012). This approach provides the most precise way to characterize the structural-functional coupling because all data are acquired in the same individual. However, the restricted multimodal data set, which could be simultaneously acquired in the same participant limits the comprehensive examination of the structural-functional coupling. No studies have collected retinotopic, connectivity, and functional data to define hMT+ at the same time in the same group of participants, let alone cytoarchitectonic measurement cannot be acquired *in vivo*. Complementary to the studies on individuals, comparing multiple atlases from different groups of participants

provide further information on the structural-functional coupling. Until now, few studies have examined the correspondence between functional hMT+ and hMT+ defined by other criteria on the group maps (i.e., atlases). Wilms et al. (2005) found a good agreement between fMRI activation and the cytoarchitecture defined hMT+ map by measuring their spatial overlap in 14 participants. Here, using large-scale fMRI localizer data, we extended their results in two aspects. First, we revealed that besides the cytoarchitectonic hMT+ atlas, the functional hMT+ atlas agreed well with the hMT+ defined based on retinotopy, connectivity, and multimodal features, suggesting good structural-functional coupling in the hMT+. Second, we revealed that the correspondences vary across atlases. The center location of the functional hMT+ atlas was largely different from that of other atlases. When the area became larger, the multimodal features-defined hMT+ showed the tightest correspondence to the functional hMT+ among the four atlases defined by other criteria (Figure 5b, dice >0.8 when area larger than 300 mm<sup>2</sup>), implying that functional activation of the hMT+ is determined by multimodal features rather than by a single feature. However, it should be noted that although hMT+ atlases based on cytoarchitecture, retinotopy, and connectivity showed similar spatial correspondence to the functional hMT+ atlas, the main axes of the configurations were different; the main axes of atlases based on retinotopy and connectivity were horizontal to the ITS, while that of the atlas based on cytoarchitecture was vertical to the ITS (similar to those of the atlases based on functional and multimodal features). One possibility is that the low SNR and small sample size used in building retinotopic ( $N = 53$ ) and connectivity ( $N = 40$ ) atlases may bias the configurations of the probabilistic maps. Future studies, which simultaneously collect the multimodal data in a large cohort of participants will shed light on the exact coupling between function and structure of the hMT+.

Unlike other hMT+ atlases (except multimodal atlas), the functional hMT+ atlas relies heavily on the macroanatomical landmark in delineating the individual hMT+. A reliable coupling has long been revealed between hMT+ and the junction between the ITS and AOS at the centimeter scale (Dumoulin et al., 2000; Watson et al., 1993; Weiner & Grill-Spector, 2011). To this end, the ITS-AOS junction was used to constrain the delineation of individual hMT+. As the junction is identifiable in almost all brains, it helped much to accurately localize the hMT+, particularly when hMT+ activation is noisy. We believe this is one of the important reasons why individual functional hMT+ showed high convergence across participants (maximum convergence, LH: 80.8%; RH: 80.6%) and why our atlas showed significant interhemispheric spatial correspondences. On the other hand, we doubt that the large interhemispheric difference from some other atlases may be caused by a lack of using a macroanatomical landmark to guide the delineation of the hMT+. Moreover, as we used the macroanatomical landmark from structural MRI in defining our atlas, our atlas can be considered as a bimodal atlas. This may be why our atlas matched well the multimodal atlas. We advocate that the macroanatomical landmark should be considered in defining the functional areas.

### 4.3 | Limitations of the present hMT+ atlas

While we have emphasized the ability of our hMT+ atlas to identify the functional hMT+, we also recognize several limitations. First, the present study used relative low spatial resolution fMRI data (voxel size = 3.1 × 3.1 × 4.8 mm<sup>3</sup>) to build the functional hMT+ atlas. The partial-volume effect from the large voxel could cause substantial spread of activation onto the bank of the sulcus and thus renders the localization of brain activity imprecise because the neighboring locations in volume space often represent locations that are distant on the cortical surface. Such “bleeding” thus may introduce some biases in defining the hMT+ and measuring its interindividual variability. High-resolution fMRI, which is more sensitive to interregional and interindividual anatomical differences, could be used to advance the localization of hMT+ in future studies. Second, only one specific motion stimulus (i.e., moving concentric rings) was used to localize the functional hMT+, which may limit the generalization of the atlas. Furthermore, the single type of motion stimulus cannot afford to distinguish the subregions of hMT+. Besides the moving concentric rings, diverse moving stimuli such as translating noise or random dot patterns have been used to map the functional hMT+. A representative hMT+ atlas, which contains detailed information of its subregions, remains to be built in the future from a large cohort of participants using multiple kinds of moving stimuli. Finally, brain structure and function develop significantly from childhood to adulthood (Casey, Giedd, & Thomas, 2000; Giedd et al., 1999; Gomez et al., 2017). Although the developmental trajectory of the hMT+ is poorly known (Taylor, Olulade, Luetje, & Eden, 2018), behavioral studies have revealed that the ability for motion perception continues to develop until 14 years of age (Joshi & Falkenberg, 2015). The atlas presented in this study was constructed from young adults within a narrow range of age (mean = 20.31 years, SD = 1.26 years). Therefore, the atlas may not be applicable to studies on people with a different age groups, especially children. Future studies are needed to construct a functional atlas that reflects the development of functional hMT+.

### 4.4 | Future uses of the hMT+ atlas in basic and translational research

Our functional hMT+ atlas showed high sensitivity in extracting motion-related responses in ROI analysis. Here, we discuss three future uses of our hMT+ atlas. First, as our hMT+ atlas captures both the population mean and the population variance of the location of the hMT+, it can be used to localize the hMT+ when fMRI data are not available, which is especially crucial in patient populations. Second, as the hMT+ has been implicated in different disorders such as akinetopsia (Shipp, de Jong, Zihl, Frackowiak, & Zeki, 1994; Zihl & Heywood, 2015), dyslexia (Rauschecker et al., 2011; Wandell & Le, 2017), and autism (Peiker et al., 2015), our hMT+ atlas has translational applications. Specifically, future studies that intend to compare the hMT+ between control and patient populations can use our atlas for accurate localization of the hMT+ in each hemisphere prior to performing the comparison between groups. Finally, as more anatomical

and functional atlases will be developed in future studies, a similar approach to ours can be implemented not just in the hMT+ but also in some other regions in which (a) SNR and sample size might affect the generation of a reliable atlas and (b) comparisons across atlases are made to examine the correspondence between areas identified by different techniques in the same cortical expanse (Van Essen et al., 2012; Van Essen & Glasser, 2018).

## 5 | CONCLUSION

We developed a probabilistic atlas of the hMT+ from large-scale functional localizer data. We found substantial interindividual variability in the location of hMT+, even though data with high tSNR and ample sample size were used. The functional atlas showed good spatial correspondence to other atlases defined based on cytoarchitecture, retinotopy, connectivity, and multimodal features, and it was more sensitive to motion-related responses than other single-feature hMT+ atlases. We made this atlas freely available for download at <http://www.brainactivityatlas.org/atlas/atlas-download> for future use.

## ACKNOWLEDGEMENTS

The authors thank Dr Kevin S. Weiner from the Department of Psychology, University of California, Berkeley for helpful discussion on the delineation of hMT+, preparation of Figure 1, and for valuable comments for the manuscript.

## CONFLICT OF INTEREST

The authors declare no potential conflict of interest.

## ORCID

Zonglei Zhen  <https://orcid.org/0000-0002-6748-6434>

Jia Liu  <https://orcid.org/0000-0003-0383-0934>

## REFERENCES

- Amano, K., Wandell, B. A., & Dumoulin, S. O. (2009). Visual field maps, population receptive field sizes, and visual field coverage in the human MT+ complex. *Journal of Neurophysiology*, 102(5), 2704–2718. <https://doi.org/10.1152/jn.00102.2009>
- Barch, D. M., Burgess, G. C., Harms, M. P., Petersen, S. E., Schlaggar, B. L., Corbetta, M., ... WU-Minn HCP Consortium. (2013). Function in the human connectome: Task-fMRI and individual differences in behavior. *NeuroImage*, 80, 169–189. <https://doi.org/10.1016/j.neuroimage.2013.05.033>
- Bennett, C. M., & Miller, M. B. (2010). How reliable are the results from functional magnetic resonance imaging? *Annals of the New York Academy of Sciences*, 1191, 133–155. <https://doi.org/10.1111/j.1749-6632.2010.05446.x>
- Blokland, G. A., McMahon, K. L., Thompson, P. M., Martin, N. G., de Zubicaray, G. I., & Wright, M. J. (2011). Heritability of working memory brain activation. *The Journal of Neuroscience*, 31(30), 10882–10890. <https://doi.org/10.1523/JNEUROSCI.5334-10.2011>
- Bridge, H., Clare, S., & Krug, K. (2014). Delineating extrastriate visual area MT(V5) using cortical myeloarchitecture. *NeuroImage*, 93 Pt. 2, 231–236. <https://doi.org/10.1016/j.neuroimage.2013.03.034>
- Casey, B. J., Giedd, J. N., & Thomas, K. M. (2000). Structural and functional brain development and its relation to cognitive development. *Biological Psychology*, 54(1–3), 241–257.
- Castelli, F., Happe, F., Frith, U., & Frith, C. (2000). Movement and mind: A functional imaging study of perception and interpretation of complex intentional movement patterns. *NeuroImage*, 12(3), 314–325. <https://doi.org/10.1006/nimg.2000.0612>
- DeYoe, E. A., Carman, G. J., Bandettini, P., Glickman, S., Wieser, J., Cox, R., ... Neitz, J. (1996). Mapping striate and extrastriate visual areas in human cerebral cortex. *Proceedings of the National Academy of Sciences of the United States of America*, 93(6), 2382–2386.
- Duecker, F., Frost, M. A., de Graaf, T. A., Graewe, B., Jacobs, C., Goebel, R., & Sack, A. T. (2014). The cortex-based alignment approach to TMS coil positioning. *Journal of Cognitive Neuroscience*, 26(10), 2321–2329. [https://doi.org/10.1162/jocn\\_a\\_00635](https://doi.org/10.1162/jocn_a_00635)
- Dumoulin, S. O., Bittar, R. G., Kabani, N. J., Baker, C. L., Le Goualher, G., Pike, G. B., & Evans, A. C. (2000). A new anatomical landmark for reliable identification of human area V5/MT: A quantitative analysis of sulcal patterning. *Cerebral Cortex*, 10(5), 454–463.
- Engell, A. D., & McCarthy, G. (2013). Probabilistic atlases for face and biological motion perception: An analysis of their reliability and overlap. *NeuroImage*, 74, 140–151. <https://doi.org/10.1016/j.neuroimage.2013.02.025>
- Fan, L., Li, H., Zhuo, J., Zhang, Y., Wang, J., Chen, L., ... Jiang, T. (2016). The human brainnetome atlas: A new brain atlas based on connectional architecture. *Cerebral Cortex*, 26(8), 3508–3526. <https://doi.org/10.1093/cercor/bhw157>
- Fischl, B., Sereno, M. I., Tootell, R. B., & Dale, A. M. (1999). High-resolution intersubject averaging and a coordinate system for the cortical surface. *Human Brain Mapping*, 8(4), 272–284.
- Frost, M. A., & Goebel, R. (2012). Measuring structural-functional correspondence: Spatial variability of specialised brain regions after macro-anatomical alignment. *NeuroImage*, 59(2), 1369–1381. <https://doi.org/10.1016/j.neuroimage.2011.08.035>
- Gauthier, I., Curran, T., Curby, K. M., & Collins, D. (2003). Perceptual interference supports a non-modular account of face processing. *Nature Neuroscience*, 6(4), 428–432. <https://doi.org/10.1038/nn1029>
- Giedd, J. N., Blumenthal, J., Jeffries, N. O., Castellanos, F. X., Liu, H., Zijdenbos, A., ... Rapoport, J. L. (1999). Brain development during childhood and adolescence: A longitudinal MRI study. *Nature Neuroscience*, 2(10), 861–863. <https://doi.org/10.1038/13158>
- Glasser, M. F., Coalson, T. S., Robinson, E. C., Hacker, C. D., Harwell, J., Yacoub, E., ... Van Essen, D. C. (2016). A multi-modal parcellation of human cerebral cortex. *Nature*, 536(7615), 171–178. <https://doi.org/10.1038/nature18933>
- Glasser, M. F., Sotiroopoulos, S. N., Wilson, J. A., Coalson, T. S., Fischl, B., Andersson, J. L., ... WU-Minn HCP Consortium. (2013). The minimal preprocessing pipelines for the Human Connectome Project. *NeuroImage*, 80, 105–124. <https://doi.org/10.1016/j.neuroimage.2013.04.127>
- Golarai, G., Ghahremani, D. G., Whitfield-Gabrieli, S., Reiss, A., Eberhardt, J. L., Gabrieli, J. D., & Grill-Spector, K. (2007). Differential development of high-level visual cortex correlates with category-specific recognition memory. *Nature Neuroscience*, 10(4), 512–522. <https://doi.org/10.1038/nn1865>
- Gomez, J., Barnett, M. A., Natu, V., Mezer, A., Palomero-Gallagher, N., Weiner, K. S., ... Grill-Spector, K. (2017). Microstructural proliferation in human cortex is coupled with the development of face processing. *Science*, 355(6320), 68–71. <https://doi.org/10.1126/science.aag0311>
- Greve, D. N., & Fischl, B. (2009). Accurate and robust brain image alignment using boundary-based registration. *NeuroImage*, 48(1), 63–72. <https://doi.org/10.1016/j.neuroimage.2009.06.060>

- Greve, D. N., Van der Haegen, L., Cai, Q., Stufflebeam, S., Sabuncu, M. R., Fischl, B., & Brysbaert, M. (2013). A surface-based analysis of language lateralization and cortical asymmetry. *Journal of Cognitive Neuroscience*, 25(9), 1477–1492. [https://doi.org/10.1162/jocn\\_a\\_00405](https://doi.org/10.1162/jocn_a_00405)
- Huk, A. C., Dougherty, R. F., & Heeger, D. J. (2002). Retinotopy and functional subdivision of human areas MT and MST. *The Journal of Neuroscience*, 22(16), 7195–7205.
- Joshi, M. R., & Falkenberg, H. K. (2015). Development of radial optic flow pattern sensitivity at different speeds. *Vision Research*, 110(Pt. A), 68–75. <https://doi.org/10.1016/j.visres.2015.03.006>
- Kolster, H., Peeters, R., & Orban, G. A. (2010). The retinotopic organization of the human middle temporal area MT/V5 and its cortical neighbors. *The Journal of Neuroscience*, 30(29), 9801–9820.
- Koten, J. W., Jr., Wood, G., Hagoort, P., Goebel, R., Propping, P., Willmes, K., & Boomsma, D. I. (2009). Genetic contribution to variation in cognitive function: An fMRI study in twins. *Science*, 323(5922), 1737–1740. <https://doi.org/10.1126/science.1167371>
- Large, I., Bridge, H., Ahmed, B., Clare, S., Kolasinski, J., Lam, W. W., ... Krug, K. (2016). Individual differences in the alignment of structural and functional markers of the V5/MT complex in primates. *Cerebral Cortex*, 26(10), 3928–3944. <https://doi.org/10.1093/cercor/bhw180>
- Malikovic, A., Amunts, K., Schleicher, A., Mohlberg, H., Eickhoff, S. B., Wilms, M., ... Zilles, K. (2007). Cytoarchitectonic analysis of the human extrastriate cortex in the region of V5/MT+: A probabilistic, stereotaxic map of area hOc5. *Cerebral Cortex*, 17(3), 562–574. <https://doi.org/10.1093/cercor/bhj181>
- Peiker, I., David, N., Schneider, T. R., Nolte, G., Schottke, D., & Engel, A. K. (2015). Perceptual integration deficits in autism spectrum disorders are associated with reduced interhemispheric gamma-band coherence. *The Journal of Neuroscience*, 35(50), 16352–16361. <https://doi.org/10.1523/JNEUROSCI.1442-15.2015>
- Polk, T. A., Park, J., Smith, M. R., & Park, D. C. (2007). Nature versus nurture in ventral visual cortex: A functional magnetic resonance imaging study of twins. *The Journal of Neuroscience*, 27(51), 13921–13925. <https://doi.org/10.1523/JNEUROSCI.4001-07.2007>
- Polley, D. B., Steinberg, E. E., & Merzenich, M. M. (2006). Perceptual learning directs auditory cortical map reorganization through top-down influences. *The Journal of Neuroscience*, 26(18), 4970–4982. <https://doi.org/10.1523/JNEUROSCI.3771-05.2006>
- Rauschecker, A. M., Bowen, R. F., Perry, L. M., Kevan, A. M., Dougherty, R. F., & Wandell, B. A. (2011). Visual feature-tolerance in the reading network. *Neuron*, 71(5), 941–953. <https://doi.org/10.1016/j.neuron.2011.06.036>
- Shipp, S., de Jong, B. M., Zihl, J., Frackowiak, R. S., & Zeki, S. (1994). The brain activity related to residual motion vision in a patient with bilateral lesions of V5. *Brain*, 117(Pt. 5), 1023–1038.
- Song, Y., Hu, S., Li, X., Li, W., & Liu, J. (2010). The role of top-down task context in learning to perceive objects. *The Journal of Neuroscience*, 30(29), 9869–9876. <https://doi.org/10.1523/JNEUROSCI.0140-10.2010>
- Taylor, C. M., Olulade, O. A., Luetje, M. M., & Eden, G. F. (2018). An fMRI study of coherent visual motion processing in children and adults. *NeuroImage*, 173, 223–239. <https://doi.org/10.1016/j.neuroimage.2018.02.001>
- Tootell, R. B., Reppas, J. B., Dale, A. M., Look, R. B., Sereno, M. I., Malach, R., ... Rosen, B. R. (1995). Visual motion aftereffect in human cortical area MT revealed by functional magnetic resonance imaging. *Nature*, 375(6527), 139–141. <https://doi.org/10.1038/375139a0>
- Tootell, R. B., Reppas, J. B., Kwong, K. K., Malach, R., Born, R. T., Brady, T. J., ... Belliveau, J. W. (1995). Functional analysis of human MT and related visual cortical areas using magnetic resonance imaging. *The Journal of Neuroscience*, 15(4), 3215–3230.
- Van Essen, D. C., & Glasser, M. F. (2018). Parcellating cerebral cortex: How invasive animal studies inform noninvasive mapmaking in humans. *Neuron*, 99(4), 640–663. <https://doi.org/10.1016/j.neuron.2018.07.002>
- Van Essen, D. C., Glasser, M. F., Dierker, D. L., Harwell, J., & Coalson, T. (2012). Parcellations and hemispheric asymmetries of human cerebral cortex analyzed on surface-based atlases. *Cerebral Cortex*, 22(10), 2241–2262. <https://doi.org/10.1093/cercor/bhr291>
- Wandell, B. A., & Le, R. K. (2017). Diagnosing the neural circuitry of Reading. *Neuron*, 96(2), 298–311. <https://doi.org/10.1016/j.neuron.2017.08.007>
- Wang, L., Mruczek, R. E., Arcaro, M. J., & Kastner, S. (2015). Probabilistic maps of visual topography in human cortex. *Cerebral Cortex*, 25(10), 3911–3931.
- Watson, J. D., Myers, R., Frackowiak, R. S., Hajnal, J. V., Woods, R. P., Mazziotta, J. C., ... Zeki, S. (1993). Area V5 of the human brain: Evidence from a combined study using positron emission tomography and magnetic resonance imaging. *Cerebral Cortex*, 3(2), 79–94.
- Weiner, K. S., & Grill-Spector, K. (2011). Not one extrastriate body area: Using anatomical landmarks, hMT+, and visual field maps to parcellate limb-selective activations in human lateral occipitotemporal cortex. *NeuroImage*, 56(4), 2183–2199. <https://doi.org/10.1016/j.neuroimage.2011.03.041>
- Wheatley, T., Milleville, S. C., & Martin, A. (2007). Understanding animate agents: Distinct roles for the social network and mirror system. *Psychological Science*, 18(6), 469–474. <https://doi.org/10.1111/j.1467-9280.2007.01923.x>
- Wilms, M., Eickhoff, S. B., Specht, K., Amunts, K., Shah, N. J., Malikovic, A., & Fink, G. R. (2005). Human V5/MT+: Comparison of functional and cytoarchitectonic data. *Anatomy and Embryology*, 210(5–6), 485–495. <https://doi.org/10.1007/s00429-005-0064-y>
- Zeki, S., Watson, J. D., Lueck, C. J., Friston, K. J., Kennard, C., & Frackowiak, R. S. (1991). A direct demonstration of functional specialization in human visual cortex. *The Journal of Neuroscience*, 11(3), 641–649.
- Zhen, Z., Yang, Z., Huang, L., Kong, X. Z., Wang, X., Dang, X., ... Liu, J. (2015). Quantifying interindividual variability and asymmetry of face-selective regions: A probabilistic functional atlas. *NeuroImage*, 113, 13–25. <https://doi.org/10.1016/j.neuroimage.2015.03.010>
- Zihl, J., & Heywood, C. A. (2015). The contribution of LM to the neuroscience of movement vision. *Frontiers in Integrative Neuroscience*, 9, 6. <https://doi.org/10.3389/fnint.2015.00006>

## SUPPORTING INFORMATION

Additional supporting information may be found online in the Supporting Information section at the end of this article.

**How to cite this article:** Huang T, Chen X, Jiang J, Zhen Z, Liu J. A probabilistic atlas of the human motion complex built from large-scale functional localizer data. *Hum Brain Mapp*. 2019;40:3475–3487. <https://doi.org/10.1002/hbm.24610>